SUPPORTING INFORMATION (SI)

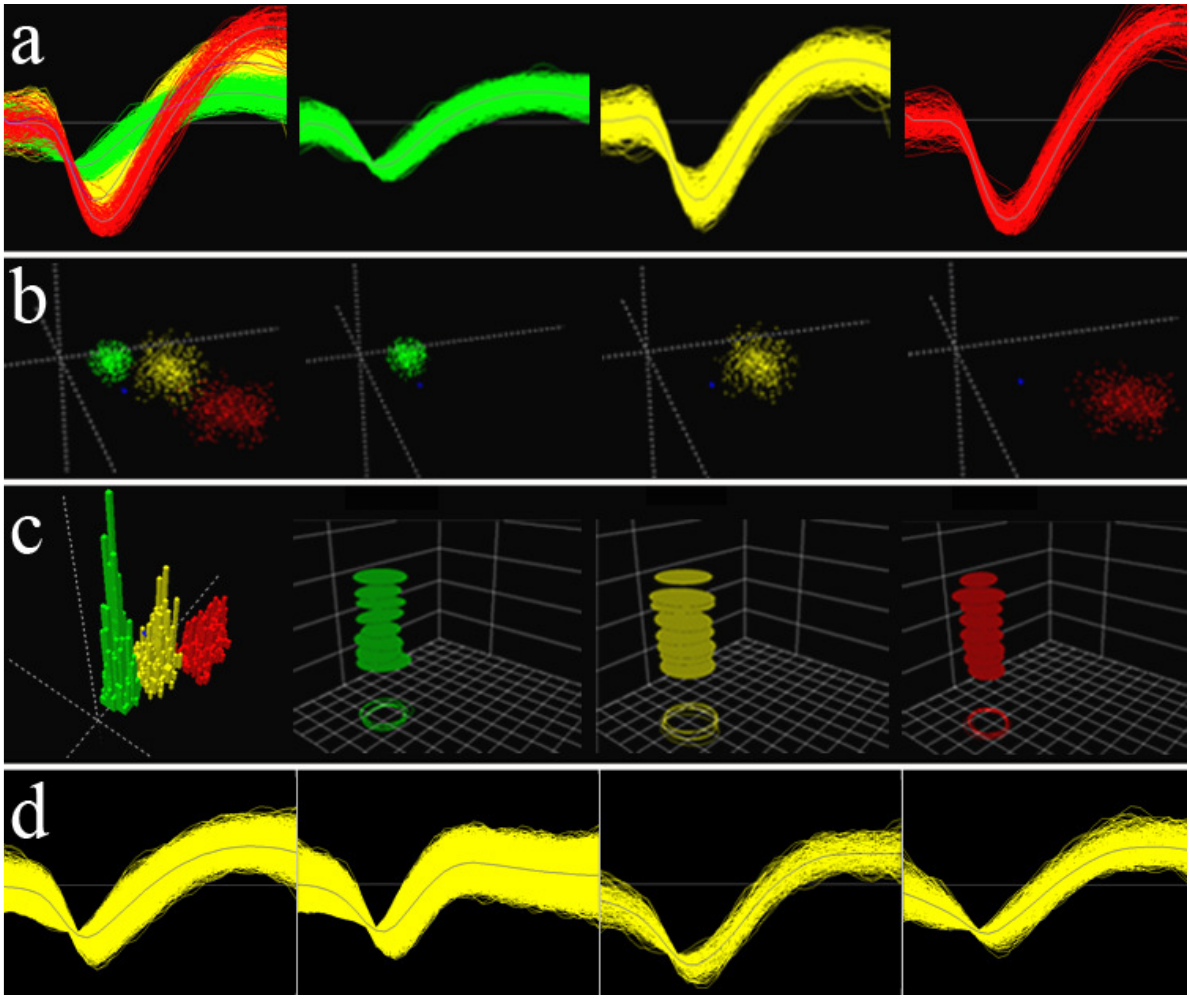

Figure S1: Example of spike isolation from one electrode. a) Three units discriminated based on their different waveform envelopes. Multielectrode arrays of single microwires allow for massive single-unit recording but some multi-unit activity may also be recorded (green waveforms). b) Waveform cluster separation in 3D principal component space. c) The panel on the left shows histograms of waveform clusters for each isolated unit. In the three panels to the right, ellipsoid superposition indicates the stability of the waveforms sampled regularly throughout the recording session (time in the z axis). d) Examples of units sorted in different channels from the same animal.

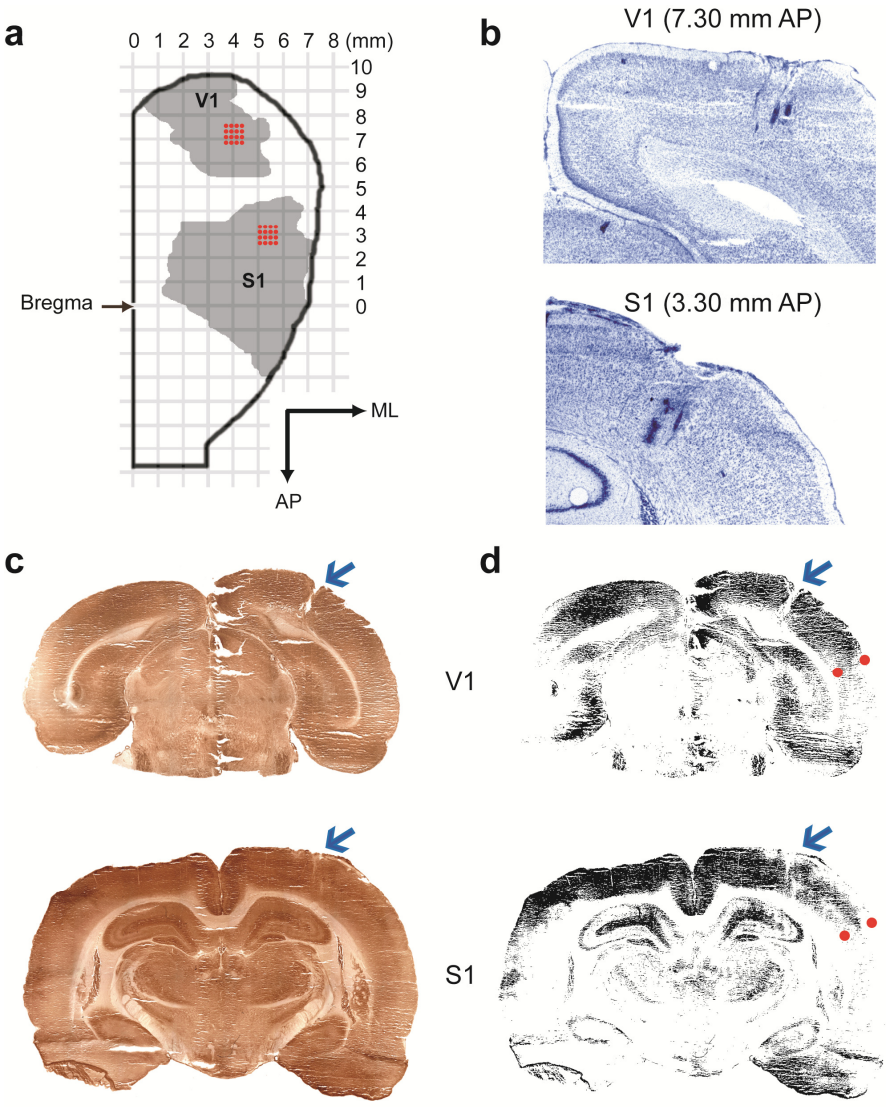

Figure S2: Placement of arrays within V1 and S1. a) The arrays targeted restricted portions of V1 and S1. AP for antero-posterior, ML for medial-lateral. Grey shading indicates the extent of V1 and S1 in stereotaxic coordinates (Paxinos, 1997). Red dots indicate array positioning. **b)** Arrays were aimed at cortical layer V (depth 1.5 mm for S1 and 1.4 mm for V1). Cresyl-stained sections were used to verify the anatomical placement and depth of the electrodes. Note the parallel tracks stained in dark blue, due to gliosis around the electrodes. **c)** Cytochrome-oxidase (CO) histochemistry was used to determine the V1 and S1 boundaries. Electrode tracks indicated by blue arrows. d) Transitions from high to low staining in thresholded CO images facilitate visualization of the V1 and S1 borders, indicated by red circles.

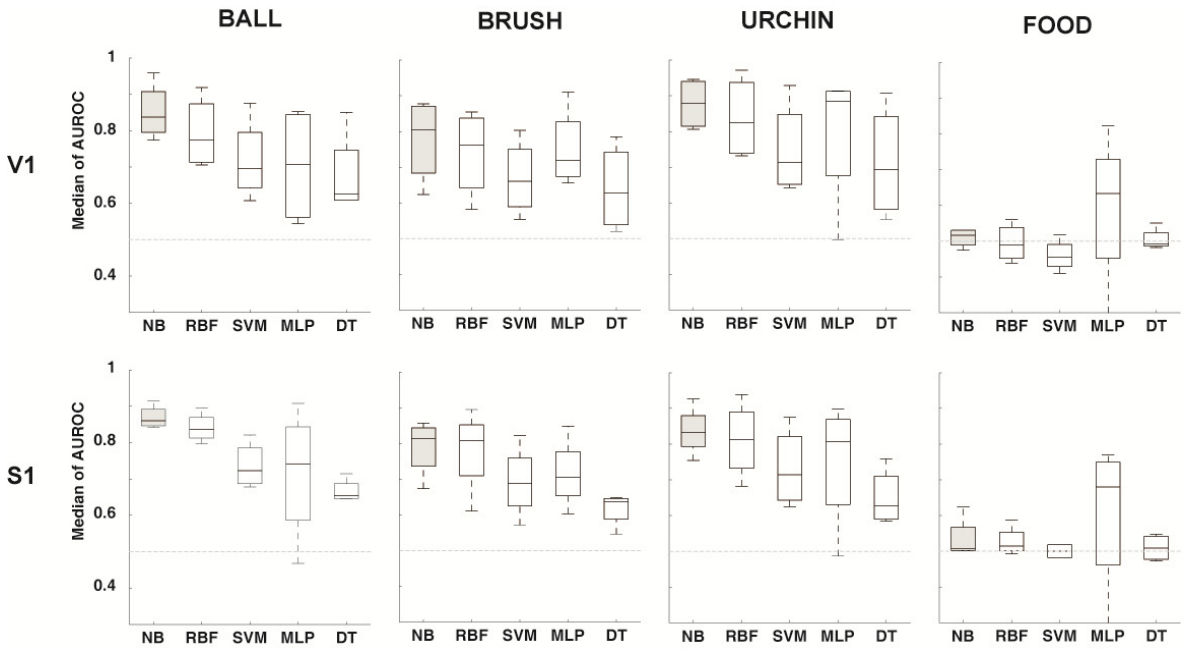

Figure S3: Object classification based on neuronal ensemble activity did not differ between V1 and S1 for any of the five binary classifier models employed. The data were analyzed with the following models: naive Bayes classifier (NB), radial basis functions (RBF); support vector machines (SVM), multilayer perceptron (MLP) and decision tree (DT). No statistically significant difference was observed between classifier models across all objects for neuronal ensembles recorded in V1 (two-tailed Wilcoxon signed-rank, $p \geq 0.1143$ with alpha corrected for 40 comparisons = 0.00125) or S1 (two-tailed Wilcoxon signed-rank $p \geq 0.0286$ with alpha corrected for 40 comparisons = 0.00125). Therefore, it is safe to assume that there is no model-related artifact.

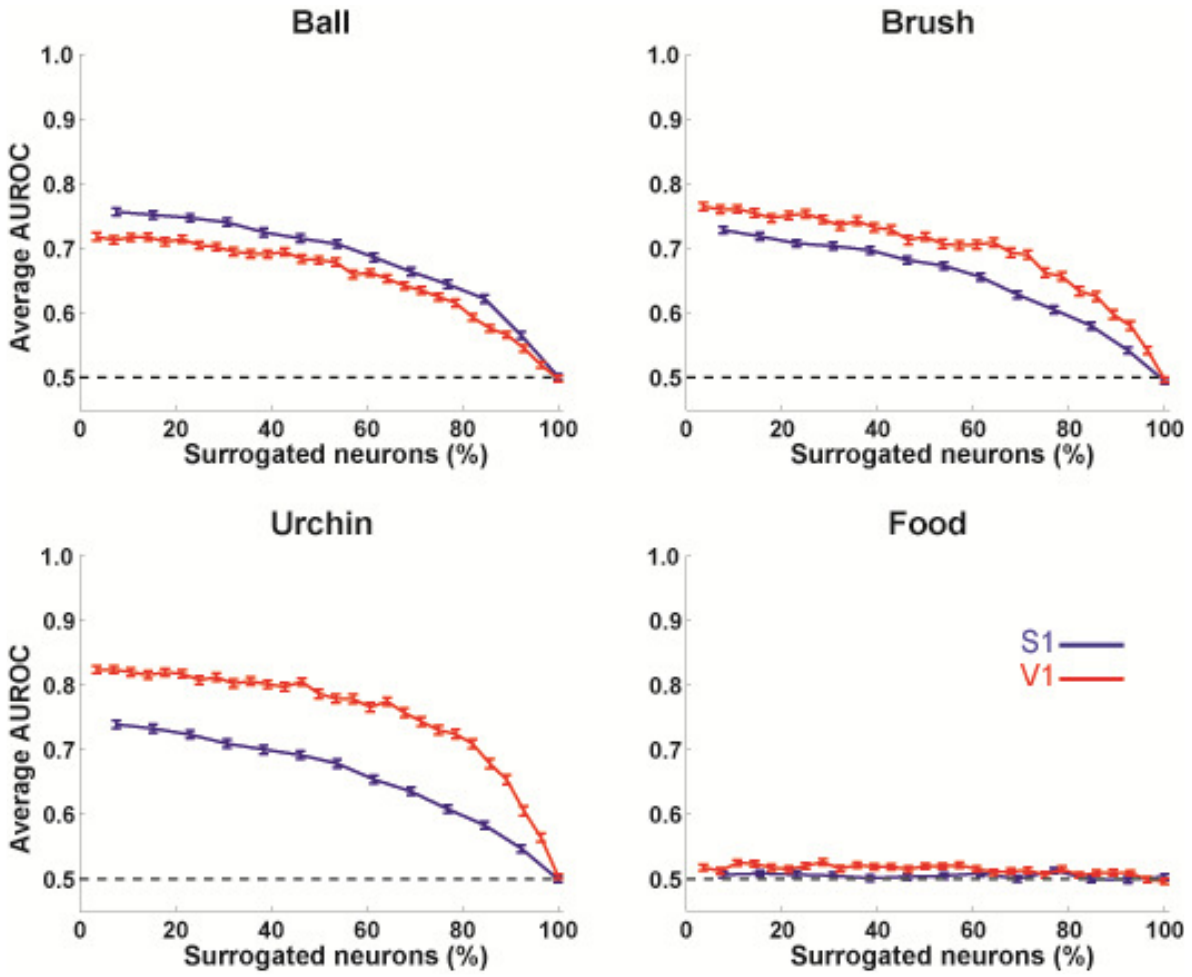

Figure S4: Poisson surrogation of the data impairs object classification. Results from a representative animal, depicting the progressive decay of AUROC values as the proportion of Poisson surrogated neurons increases.

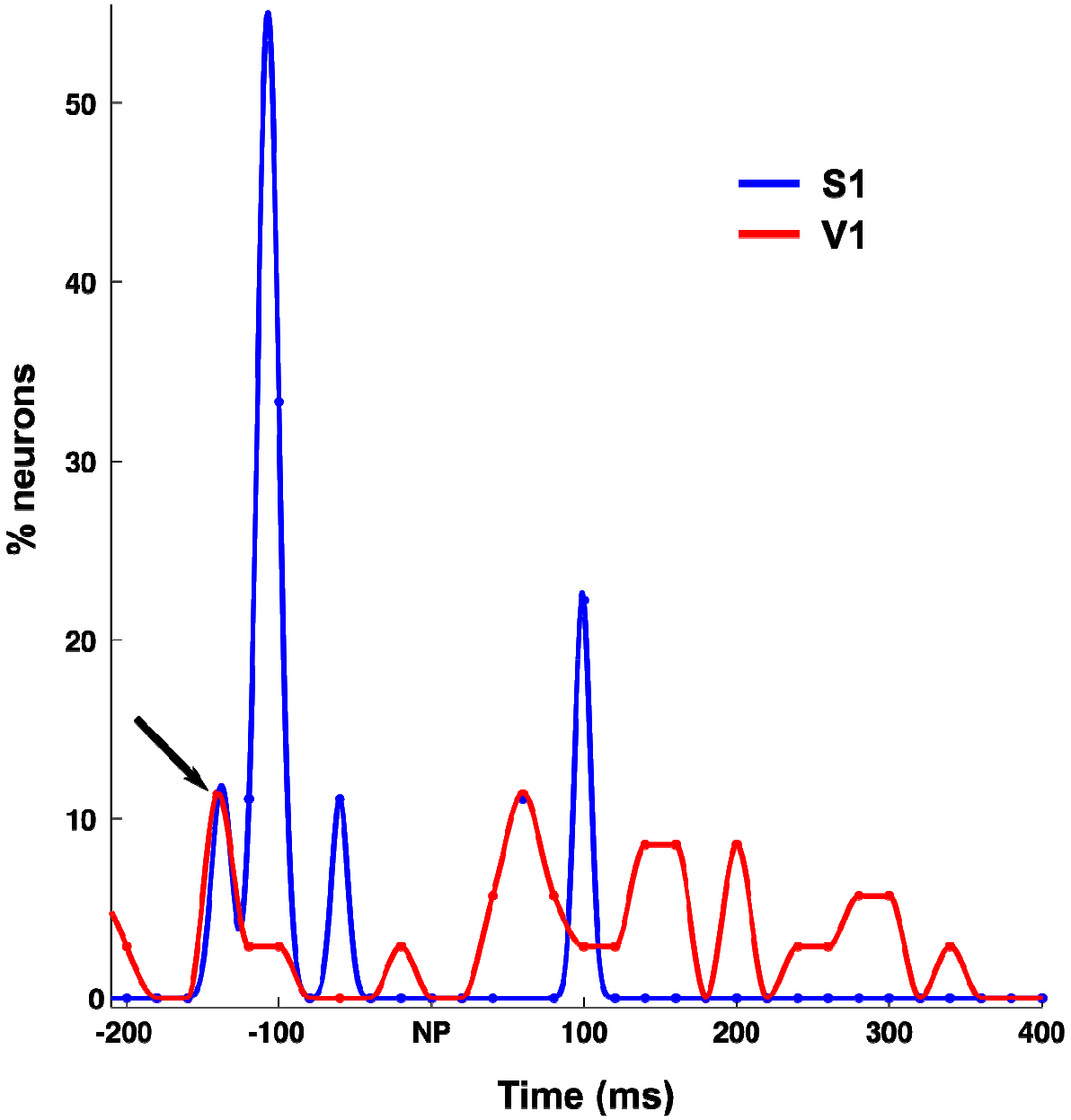

Figure S5: Distribution of latencies for S1 and V1 responses in the tactile discrimination task. In V1, latencies are widely distributed and in average larger than latencies in S1. Notice however that the early peak indicated by the arrow was identical for these areas.

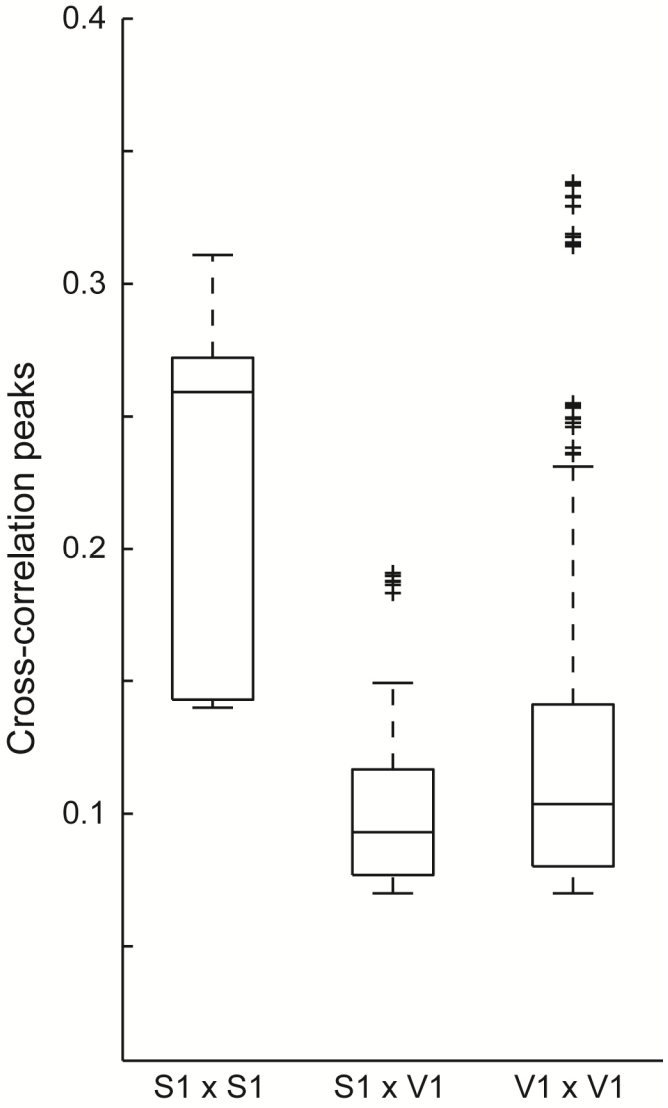

Figure S6: Cross-correlations around NP (± 300ms), within and across primary sensory areas. To address the issue of change in cross-correlations as a function of distance from S1, we calculated cross-correlations (1) for neuronal pairs recorded across electrodes within the same area (intra-area long-range interactions, 0.25-1 mm apart) or across the S1/V1 areas (inter-area very long range interactions, 3.3-5.6 mm apart). Cross-correlations were higher for S1 x S1 neuronal pairs than for V1 x V1 or V1 x S1 neuronal pairs (Wilcoxon test, $p<<0.01$), i.e. synchrony decays as the distance from S1 increases, as previously shown in monkeys subjected to tactile stimulation (2).

Supporting Methods 1: Electrophysiological recordings. After 1-week recovery from surgery, animals were recorded under various conditions. Continuous extracellular recordings were performed for up to 6 hours using a software package for supervised real-time spike sorting (SortClient 2002, Plexon Inc, USA). Up to 4 templates per channel were sorted online and validated offline to detect spikes (Offline Sorter 2.3, Plexon Inc, USA) using the following cumulative criteria: a) voltage thresholds > 3 standard deviations of amplitude distributions; b) signal-to-noise ratio >2.5 (as verified on the oscilloscope screen); c) less than 0.5% of inter-spike intervals (ISI) smaller than 1.0 ms; d) stereotypy of waveform shapes, as determined by a waveform template algorithm and principal component analysis. Behaviors were continuously recorded under visible or infrared light with a CCD camera connected to a videotracking system (Cineplex) synchronized to the neural recordings. Illuminance in the visible spectrum was measured inside the recording chambers with lights off using a Minipa Electronics luximeter, model MLM - 1011.

Supporting Methods 2: Histological confirmation of electrode placement. After recordings animals were killed with pentobarbital, and the brains were removed, quickly frozen in embedding medium (Tissue Tek, Sakura Finetek, USA), frontally sectioned at 50 μm in a criostat (Micron HM 550, Germany) and thaw-mounted following a serial distribution over glass slides (Super Frost Plus - VWR International, USA). The brains were frozen fresh and post-fixed after sectioning. To reveal cytochrome oxidase activity (3), brain sections were washed in 0.1M phosphate buffer (PB) during 10 min and incubated in a solution containing 0.05% diaminobenzidine (DAB), 0.03% cytochrome c and 0.02% catalase in 0.1M PB (Sigma Company, USA). The reaction was monitored every 30 min and was interrupted by washing sections in 0.1M PB. Alternate sections were stained with cresyl violet. Sections were dehydrated and coverslipped with Entellan (Merck, Germany). The anatomical placement of individual electrodes within target areas was confirmed by histological reconstruction of electrode tracks in cresyl-stained sections. The boundaries of V1 and S1 were determined by the transition between high and low cytochrome-oxidase staining. The mapping and superposition of electrode tracks and cytochrome-oxidase rich areas was performed using a Neurolucida system (MBF Bioscience Inc., USA).

Supporting Methods 3: Free exploration of novel objects. Objects for tactile exploration were constructed from toys and raw materials, and the movie for visual exploration was generated using scenes of other rats feeding and exploring. Free exploration sessions lasted 10-20 min; pre and post-exposure periods of up to 6 hours were recorded, as previously described (4). LFP spectral maps for the separation of waking and sleep states were employed to sort waking periods (5). Times of contact between whiskers and objects were determined by slow-motion inspection of video recordings.

Supporting Methods 4: Statistical analysis of spike responses. In animals subjected to object exploration in the dark or exposed to movie presentation, spike trains were subjected to Kruskal-Wallis comparisons calculated for 10 min intervals before and after stimulus with alpha=0.05. Spike trains identified as modulated by the stimulus were then subjected to a post-hoc two-tailed Wilcoxon signed-rank test with alpha corrected within each animal

for the total number of S1 and V1 neurons that reached significance in the Kruskal-Wallis test. In animals subjected to the tactile discrimination task (range 69-102 trials), we used 500ms intervals before and after the breaking of an infrared discrimination beam positioned to mark the initial contact of the whiskers with the metal bars. For the cumulative sum analysis, we used the Neuroexplorer software (Plexon Inc., USA) to identify statistically significant responses from the PSTHs using cumulative deviations from baseline firing rates (6-9). To identify the onsets of significant deviations, we calculated the deviation of the poststimulus cumulative summed firing rate from the expected cumulative sum, based on the average baseline firing rate. The latency to the first peak was used to determine the onset time of the response. In animals subjected to the tactile discrimination task, 500ms periods with respect to the nose poke were considered for the cumulative sum analysis.

Supporting Methods 5: Data preparation for binary classifiers. From any given electrode, up to 4 neurons can be recorded. All neurons recorded from V1 or S1 were pooled together, yielding N neurons. Let $\mathbf{r}_n$ denote the response of the n neuron (n=1,...,N) throughout the time observed, where each element on $\mathbf{r}_n$ denotes the time in which an action potential occurred on neuron n. For the spike data, we explored a family of codes based on spike counting (10) in successive bin sizes w. This parameter controls the time resolution of the code; its default value on this study is w=*250ms*. Having defined the bin size w, each neuron contributes W bins to the input data matrix. For a given animal, the k-th time interval of contact with an object, I_k, is defined by $I_k = [a_k, b_k]$. If $(W.w) \leq (b_k - a_k)$, it is possible to make more than one sample from that contact interval, so the next samples are built sliding (by w seconds) into interval I_k. If $(W.w) > (b_k - a_k)$, then the interval, I_k, is too short and cannot be used as input data for the given bin size w. Therefore, using the spike counting to define the code, given an interval, $I_k = [a_k, b_k]$, where $(W.w) \leq (b_k - a_k)$, and a given neuron n, we define the response vector $\mathbf{r}(a_k, b_k)$ as $\mathbf{r}(a_k, b_k) = \mathbf{h}(\boldsymbol{u}_n, w, a_k, b_k) = [\, r_0 \;\; r_1 \;\; \ldots \;\; r_l]$, where: $\boldsymbol{u}_n$, is a vector which stores the firing times of the neuron n; $\mathbf{h}$ is defined as the histogram (11) of the vector $\boldsymbol{u}_n$, between a_k and b_k, using as bin size w; and l is the number of bins on that given interval, I_k, which can be computed by $l = (b_k - a_k)/w$. Given W, as the time length of the observation, the input data samples from $\mathbf{r}(a_k, b_k)$ are obtained by taking all consecutive W-width vectors from $\mathbf{r}(a_k, b_k)$. These samples were used as input data to the decoding classifier. When considering the responses of multiple electrodes, we concatenated the corresponding response samples and used the result as input to the classifier (12). Therefore, the input data dimensionality to the classifier is $W.N$, where N is the number of neurons used to build the input data. Depending on the analysis, and the animal, we used N=1,..,144 neurons. For training and testing, the data were always divided into a training set and a test set, using always the same number of samples for all animals. In all cases the training set comprised 70% of the available contact samples of each object, while the test set included the remaining 30%. Positive samples for a given object comprise moments when the animal was in contact with that object, and negative samples for a given object are moments in which the animal was in contact with other objects. The training and test sets were built using M positive samples and 2.M negative samples, randomly chosen from all available samples.

Supporting Methods 6: Surrogated datasets. The Poisson point process (13) is well

established as a model of neuronal firing (14-16), and was used to surrogate our spike datasets. Given a neuron *n*, the approach used to surrogate the original pattern of neuronal activation was to replace the original spike counts within each 250ms bin by random firing following a Poisson distribution with the same mean found in the original samples. Figure S4 shows that average AUROC decays as the percentage of surrogated neurons increases.

Supporting Methods 7: Object recognition under different sensory conditions. Rats were handled for 4 consecutive nights, then exposed to 4 identical novel objects on the 5th night for 10 minutes, placed in the home cage for 10 minutes, and tested for 10 minutes with two identical familiar objects and two identical novel objects. The objects with different shapes and visual appearances comprised a mug and an ice-cream cup. Soda cans with different colors served as objects with identical shapes and different visual appearances. The experimental design adopted allowed for a comparison of the relevant sensory conditions without having to resort to the removal of sensory organs, which triggers major plastic changes in the brain (17) and may jeopardize spontaneous exploratory behavior (18). Interestingly, in the visuo-tactile condition rats explored for longer periods of time but discrimination was only marginally better than in the tactile-only condition (compare the first and second panels in Fig. 4; $p=0.0001$ for discrimination ratio in both cases, calculated by dividing the time spent in exploration of novel objects by the time spent in exploration of familiar objects).

Supporting Methods 8: Tactile discrimination task. Animals were submitted to an automated task for the tactile discrimination of wide and narrow apertures defined by two metal bars lateral to the whisker pads, randomly repositioned at every trial (9, 19-20). Water-deprived animals were trained over 10-20 days to learn to poke their nose through the center of an aperture and then report behaviorally the relative width of this opening, in exchange for liquid reward offered at a left or right dispenser hole depending on whether the aperture was "wide" or "narrow". Animals were trained to perform above 80% of correct trials per session before surgery, and re-trained to that level before neural recordings began. The temporal references recorded in each trial comprised the opening of the central door (CD), a nose-poke infrared beam (NP) placed inside a hole placed between the two metal bars, and reward delivery (RW). Typically, well-trained animals performed ~100 trials per session.

Supporting Methods 9: Cross correlations. Pairwise neuronal cross-correlations were calculated using 100ms sliding windows around different trial epochs (CD, NP, RW). Units from the same electrode were not considered. Results were compared for S1, V1, and S1 x V1 neuronal pairs. Normalized correlations were obtained from the paradiagonals of the normalized joint PSTHs matrices. These matrices were obtained from raw joint PSTHs by subtracting their cross-product, and then dividing by the product of the two corresponding standard deviations (1). Significance was set at two standard deviations from peak correlations obtained with shuffled data (all spikes shuffled according to a uniform distribution, 20 shuffles per neuronal pair). Only significant peak cross-correlations between 0.07 and 0.4 were considered.

Supporting References

1. Aertsen AMHJ, Gerstein GL, Habib MK, & Palm G (1989) Dynamics of neuronal firing correlation: modulation of "effective connectivity". *J Neurophysiol* 61(5):900-917.
2. Reed JL*, et al.* (2008) Widespread spatial integration in primary somatosensory cortex. *Proc Natl Acad Sci U S A* 105(29):10233-10237.
3. Hevner RF, Liu S, & Wong-Riley MT (1995) A metabolic map of cytochrome oxidase in the rat brain: histochemical, densitometric and biochemical studies. *Neuroscience* 65(2):313-342.
4. Ribeiro S*, et al.* (2007) Novel experience induces persistent sleep-dependent plasticity in the cortex but not in the hippocampus. *Frontiers in Neuroscience* 1(1):43-55.
5. Gervasoni D*, et al.* (2004) Global forebrain dynamics predict rat behavioral states and their transitions. *J. Neurosci.* 24(49):11137-11147.
6. Armstrong-James M & Fox K (1987) Spatiotemporal convergence and divergence in the rat S1 "barrel" cortex. *J Comp Neurol* 263(2):265-281.
7. Nicolelis MA & Chapin JK (1994) Spatiotemporal structure of somatosensory responses of many-neuron ensembles in the rat ventral posterior medial nucleus of the thalamus. *J Neurosci* 14(6):3511-3532.
8. Sachdev RN & Catania KC (2002) Receptive fields and response properties of neurons in the star-nosed mole's somatosensory fovea. *J Neurophysiol* 87(5):2602-2611.
9. Pantoja J*, et al.* (2007) Neuronal activity in the primary somatosensory thalamocortical loop is modulated by reward contingency during tactile discrimination. *J Neurosci.* 27(39):10608-10620.
10. Dayan P & Abbott LF (2001) *Theoretical Neuroscience: Computational and Mathematical Modeling of Neural Systems* (MIT Press, Boston).
11. Brown EN, Kass RE, & Mitra PP (2004) Multiple neural spike train data analysis: state-of-the-art and future challenges. *Nat Neurosci* 7(5):456-461.
12. Hung CP, Kreiman G, Poggio T, & DiCarlo JJ (2005) Fast readout of object identity from macaque inferior temporal cortex. *Science* 310(5749):863-866.
13. Papoulis A (1991) *Probability, Random Variables and Stochastic Processes.* (McGraw-Hill, New York) 3rd Ed.
14. Kass JH, Jain N, & Qi H (2001) The organization of the somatosensory system in primates. *The Somatosensory System: Deciphering the Brain's Own Body Image,* Methods and New Frontiers in Neuroscience, (CRC, Boca Raton), pp 1-26.
15. Amarasingham A, Chen TL, Geman S, Harrison MT, & Sheinberg DL (2006) Spike count reliability and the Poisson hypothesis. *J Neurosci* 26(3):801-809.
16. Gerstner W & Kistler WM (2002) *Spiking Neuron Models.* (Cambridge University Press, Madrid) 1st Ed.
17. Kaas JH (1991) Plasticity of sensory and motor maps in adult mammals. *Ann Rev Neurosci* 14:137-167.
18. Meyer ME (1992) The effects of bilateral and unilateral vibrissotomy on behavior within aquatic and terrestrial environments. *Physiol Behav* 51(4):877-880.

19. Krupa DJ, Matell MS, Brisben AJ, Oliveira LM, & Nicolelis MA (2001) Behavioral properties of the trigeminal somatosensory system in rats performing whisker-dependent tactile discriminations. *J Neurosci* 21(15):5752-5763.
20. Krupa DJ, Wiest MC, Shuler MG, Laubach M, & Nicolelis MAL (2004) Layer specific somatosensory cortical activation during active tactile discrimination. *Science* 304:1989-1992.